


## Anomalous Floquet tunneling in uniaxially strained graphene

Yonatan Betancur-Ocampo <sup>1,\*</sup> Parisa Majari <sup>1,†</sup> Diego Espitia <sup>1,‡</sup> François Leyvraz <sup>1,2,§</sup> and Thomas Stegmann <sup>1,||</sup>

<sup>1</sup>*Instituto de Ciencias Físicas, Universidad Nacional Autónoma de México, Cuernavaca 62210, México*

<sup>2</sup>*Centro Internacional de Ciencias, Cuernavaca 62210, México*

 (Received 30 November 2020; revised 28 January 2021; accepted 15 April 2021; published 29 April 2021)

The interplay of strain engineering and photon-assisted tunneling of electrons in graphene is considered for giving rise to atypical transport phenomena. The combination of uniaxial strain and a time-periodic potential barrier helps to control the particle transmission for a wide range of tunable parameters. With the use of the tight-binding approach, the elasticity theory, and the Floquet scattering, we find an angular shift of the transmission maximum in the sidebands for uniaxial strains breaking the mirror symmetry with respect to the normal incidence, which is called anomalous Floquet tunneling. This strain also modulates the transmission maximum in the sidebands and favors photoinduced currents. From Floquet scattering theory, we derive a generalized Snell's law for electrons in the presence of time-periodic potentials and uniaxial strain. We show that electron tunneling depends strongly on the barrier width, incident angle, uniaxial strain, and the tuning of the time-periodic potential parameters. An adequate modulation of the barrier width and oscillation amplitude serves to select the transmission in the sidebands. These findings can be useful for controlling the electron current through the photon-assisted tunneling being used in multiple nanotechnological applications.

DOI: [10.1103/PhysRevB.103.155433](https://doi.org/10.1103/PhysRevB.103.155433)

### I. INTRODUCTION

Photon-assisted tunneling is a powerful tool for controlling electron current in a device through the illumination of a particular area of the system [1–24]. The tuning of the laser frequency and the intensity can serve to explore different features in quantum transport. The understanding of the interaction of electrons under external electromagnetic fields has led to a huge number of technological applications. Nevertheless, there are many unusual electronic transport effects in the presence of time-periodic potentials that require an exhaustive study and revision from the new perspective given by the rising of two-dimensional materials [25–33]. Most of these materials belong to the classification of Dirac matter, where the Dirac-Weyl equation describes the dynamics of low-energy excitations [25,28,34–42]. With that, the Floquet scattering formalism has been the most recurrent theory for depicting the dynamics of photon-assisted tunneling [43–47]. This approach allows a simplified vision of electron tunneling through sidebands. Electrons impinging the oscillating potential barrier are reflected or refracted from different energy channels by the absorption or emission of one or multiple photons [43,48–50,52–57]. In this way, Floquet scattering has been used successfully for explaining the constructive interference of continuum and bound states in quantum wells, an effect known as Fano resonances [58–64]. Other interesting phenomena have been predicted based on the Floquet scatter-

ing theory, among them the Hartman effect [65], suppression of Klein tunneling [23,49,66,67], Floquet topological insulators [47,68–75], non-Hermitian Floquet invisibility [76], and photoelectronic-induced emission [77–79].

The interplay between strain engineering and photon-assisted tunneling may open more possibilities due to the increment of external variables to control the electron tunneling. By applying strain in graphene and related materials, the electronic band structure is modified drastically and serves to modulate the electronic, optical, and transport properties [80–100]. Inhomogeneous strain gave rise to the emergence of valleytronics and pseudomagnetic fields [92,93,101–106]. Outstanding electron optics-like effects appear in uniaxially strained graphene [34,107]. Such a system displayed partial positive refraction in asymmetric Veselago lenses, a negative reflection of electrons, and anomalous Klein tunneling [31,107,108]. Those theoretical results may be tested not only in uniaxially strained graphene, but also hexagonal optical lattices and photonic crystals [72,102,109]. Recently, a time-periodic potential in optical lattices was experimentally realized in [72]. Photonic crystal emulations of strained graphene evidenced that Klein tunneling persists for deformations along the zig-zag and armchair directions [110].

In this paper, we show that the combination of photon-assisted tunneling and strain engineering present singular transmission effects. The application of uniaxial strain causes anisotropy in the electron tunneling. Dependent on the amplitude of time-periodic potential and frequency, there are preferential incidence angles for electron tunneling in the sidebands. The electron tunneling presents an angular shift and a nontrivial modulation of the transmission maximum in the sidebands. The angular deviation of the transmission maximum has a linear behavior for tensile strains up to 10%. This new phenomenon, the anomalous Floquet tunneling,

\*ybetancur@icf.unam.mx

†majari@icf.unam.mx

‡despitia@icf.unam.mx

§leyvraz@icf.unam.mx

||stegmann@icf.unam.mx

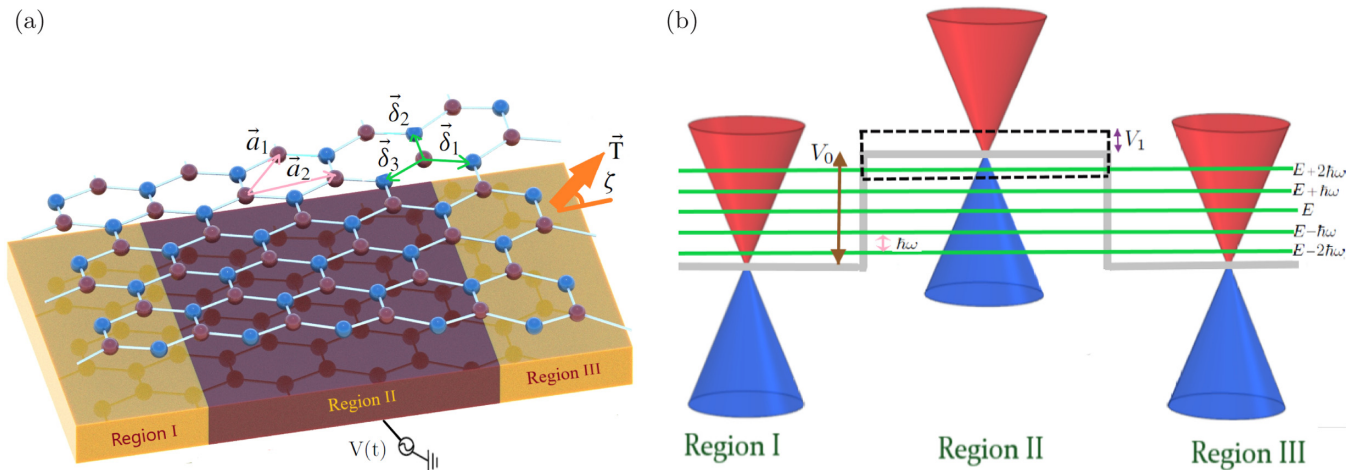


FIG. 1. (a) Schematic representation of uniaxially strained graphene in a time-periodic potential. Violet and blue circles indicate the sites of triangular sublattices  $A$  and  $B$ , respectively. The vector  $\mathbf{T}$  corresponds to the applied tension in the  $\zeta$  direction. Each nearest-neighbor possesses a hopping parameter  $\tau_j$  and bond length  $\delta_j$ . The quantities  $\mathbf{a}_1$  and  $\mathbf{a}_2$  are the deformed lattice vectors. The external gates induce a time-periodic potential barrier in region II. (b) Description of the Floquet scattering across the time-periodic potential and Dirac cone structure. Horizontal green lines represent the energy channels  $E - m\hbar\omega$ , where transmission in the sidebands occur.

evidences the role of pseudospin conservation in tunneling processes that involve time-dependent potentials and strain effects. Moreover, the tuning of the potential barrier width or the oscillating potential amplitude serves to select and improve the transmission in sidebands to produce a photoinduced electronic current. We also derive the electron optics laws using the conservation of linear momentum and sidebands energies, which evidence unusual transport effects such as sideband-dependent negative reflection due to the interplay of strain-engineering and Floquet physics.

The paper is structured as follows. In Sec. II, we give a short review of how the tight-binding approach and elasticity theory is useful for the development of a strain-modified Hamiltonian in graphene and related anisotropic hexagonal lattices. In Sec. III, we apply the Floquet scattering theory to analyze the transmission features of a fully strained graphene sheet and electron optics laws under time-periodic potential barrier. We present in Sec. IV the results of our numerical and analytical calculations of the transmission probabilities for the sidebands. We expose the conclusions and final remarks in Sec. V.

## II. DIRAC-WEYL HAMILTONIAN OF UNIAXIALLY STRAINED GRAPHENE

Uniaxially strained graphene and anisotropic hexagonal lattices are composed by two deformed triangular sublattices  $A$  and  $B$  with a basis of two atoms per unit cell, as shown in Fig. 1(a). According to the elasticity theory, the application of a uniaxial strain deforms the lattice vectors in the pristine configuration, and they are given by [34,80,107]

$$\begin{aligned} \mathbf{a}_1 &= (a_{1x}, a_{1y}) = \sqrt{3}a(1 + \rho^-\epsilon + \rho^+\epsilon \cos 2\zeta, \rho^+\epsilon \sin 2\zeta), \\ \mathbf{a}_2 &= (a_{2x}, a_{2y}) = \frac{\sqrt{3}}{2}a[1 + \rho^-\epsilon + 2\rho^+\epsilon \cos(2\zeta - 60^\circ), \\ &\quad \sqrt{3}(1 + \rho^-\epsilon) + 2\rho^+\epsilon \sin(2\zeta - 60^\circ)], \end{aligned} \quad (1)$$

where the constants  $\rho^\pm$  are defined as

$$\rho^\pm = \frac{1}{2}(1 \pm \nu) \quad (2)$$

and  $\nu = 0.18$  is the Poisson ratio, while  $a = 0.142$  nm is the bond length in pristine graphene [25]. The vectors  $\delta_j$  with  $j = 1, 2$ , and  $3$  indicate the three nearest neighbors' site on the underlying sublattice  $A$ , as shown in Fig. 1(a). The strain parameters  $\epsilon$  and  $\zeta$  quantify the percentage of tensile strain and the direction of the applied tension  $\mathbf{T}$  with respect to the  $x$  axis. The failure strain has been estimated to occur at the approximated value  $\epsilon \approx 28\%$  [111,112]. However, we use a moderated range of  $\epsilon$  from 0 to 10% in all our calculations within the linear elastic regimen, where tight-binding (TB) and density functional theory (DFT) calculations were demonstrated to have a good agreement [83]. Nevertheless, controlled and reversible extreme strains  $\epsilon > 10\%$  have been realized experimentally [113]. Using the TB approach to first nearest neighbors, we consider one orbital per atom in the unit cell and neglect the overlap orbital among neighboring sites. The scaling rule  $\tau_j = \tau \exp[-\beta(\delta_j/a - 1)]$  relates the hopping parameters  $\tau_j$  with the deformed bond lengths  $\delta_j$ . In graphene,  $\beta = 2.6$  is the Grüneisen constant and  $\tau = 2.7$  eV is the isotropic hopping [25,114]. This scaling rule evidences that the Fermi velocity is anisotropic and has a tensorial character. In the Fourier basis and expanding around the Dirac cone, the Hamiltonian is [34,107]

$$H_D = \hbar \begin{bmatrix} 0 & \mathbf{v}^{c*} \cdot \mathbf{k} \\ \mathbf{v}^c \cdot \mathbf{k} & 0 \end{bmatrix}, \quad (3)$$

where  $\mathbf{k} = (k_x, k_y)$  is the wave vector and

$$\mathbf{v}^c = (v_x^c, v_y^c) = \frac{i}{\hbar} (\mathbf{a}_1 \tau_1 e^{-i\mathbf{K}_D \cdot \delta_1} + \mathbf{a}_2 \tau_2 e^{-i\mathbf{K}_D \cdot \delta_2}), \quad (4)$$

are the complex velocities, being  $\mathbf{K}_D$  the Dirac point position, which is the solution of

$$\sum_{j=1}^3 \tau_j e^{-i\mathbf{K}_D \cdot \delta_j} = 0. \quad (5)$$

The Hamiltonian (3) is the Dirac-Weyl type  $H = v_{ij}\sigma_i p_j$ , where  $v_{ij}$  is the Fermi velocity tensor and  $p_j = \hbar k_j$  are the components of linear momentum. The electronic band structure of anisotropic hexagonal lattice, in the semimetallic phase, present generally elliptical and rotated Dirac cones. The dispersion relation

$$E = s\hbar|v^c \cdot \mathbf{k}| \quad (6)$$

of the Hamiltonian (3) displays this cone around the Dirac point in the reciprocal space, where  $s$  is the band index [107]. The eigenstates of the Dirac-Weyl-like Hamiltonian (3) have the form

$$\Phi_{s,\mathbf{k}}(\mathbf{r}) = \frac{1}{\sqrt{2}} \begin{pmatrix} 1 \\ s e^{i\phi(\mathbf{k})} \end{pmatrix} e^{i\mathbf{k}\cdot\mathbf{r}} \quad (7)$$

and the definition of pseudospin angle  $\phi(\mathbf{k})$  is

$$\tan \phi(\mathbf{k}) = \frac{-v_x k_x \sin \mu_x + v_y k_y \sin \mu_y}{v_x k_x \cos \mu_x + v_y k_y \cos \mu_y}, \quad (8a)$$

$$v_x^c = v_x e^{-i\mu_x}, \quad (8b)$$

$$v_y^c = v_y e^{i\mu_y}. \quad (8c)$$

Here  $v_{x,y}^c$  are the  $x$ - and  $y$ -components of the complex vector  $v^c$  with norm  $v_{x,y}$  and phase  $\mu_{x,y}$ . The pseudospin direction, wave vector, and the group velocity are generally not parallel.

The direction of group velocity is found to be [107]

$$\tan \theta = \frac{v_y^2 k_y + v_x v_y k_x \cos(\mu_x + \mu_y)}{v_x^2 k_x + v_x v_y k_y \cos(\mu_x + \mu_y)} \quad (9)$$

and allows to obtain the wave vector in terms of incidence angle. The application of uniaxial strains out of the zig-zag and armchair direction have led to the emergence of anomalous Klein tunneling [107], which occurs at the incidence angle

$$\theta_{KT} = \arctan[v_y \cos(\mu_x + \mu_y)/v_x] \quad (10)$$

when  $k_y = 0$  in Eq. (9).

We now rewrite the dispersion relation (6) in the more explicit form

$$E = s\hbar \sqrt{k_x^2 v_x^2 + 2k_x k_y v_x^2 \tan \theta_{KT} + k_y^2 v_y^2}. \quad (11)$$

In the next sections, we shall evidence that this symmetry breaking with respect to the  $x$  axis modifies drastically the electron transmission for the sidebands.

### III. PHOTON-ASSISTED TUNNELING THROUGH A TIME-PERIODIC POTENTIAL BARRIER

We study the tunneling of electrons in uniaxially strained graphene under the presence of a time-periodic potential barrier, as shown in Fig. 1. The photon-assisted mechanism, such as a time-periodic potential used here, causes the appearance of many sidebands [43,49,66]. These sidebands correspond to multiple copies of the dispersion relation with a relative energy separation  $\hbar\omega$ , where  $\hbar$  and  $\omega$  is the Planck constant and the potential frequency, respectively. The Floquet scattering is the usual theory to describe the tunneling of a single electron with energy  $E$  to cross the time-periodic potential gaining or losing the energy quantity  $m\hbar\omega$ , where  $m = 0, \pm 1, \pm 2, \dots$

indicates the sideband [see Fig. 1(b)]. The tunneling is elastic (inelastic) if the electron crosses the oscillating barrier without (with) changes in the energy. Most of the experimental realizations that involved photon-assisted tunneling are observed generally in the frequency range from the microwave to infrared electromagnetic spectrum [1,9,11,14,17–21,24,73,74,78,79].

We have several external variables to control the electron tunneling by means of the application of uniaxial strain and tuning of amplitude, frequency, barrier height, and width of the time-periodic potential. From a general point to view, we write the time-dependent Schrödinger equation as

$$[H(\mathbf{p}) + V(\mathbf{r}, t)]\psi(\mathbf{r}, t) = i\hbar\partial_t\psi(\mathbf{r}, t), \quad (12)$$

where  $H(\mathbf{p})$  can be a general Hamiltonian that depends only on the linear momentum  $\mathbf{p}$ . Therefore, the following development from Eqs. (12) to (18) can be applied to multiple systems in condensed matter to depict the Floquet scattering of electrons in the presence of a time-periodic potential barrier.

The eigenvectors of  $H(\mathbf{p})$  are the wave functions  $\Phi_{s,\mathbf{k}}(\mathbf{r})$  of the electron belonging to the momentum  $\mathbf{k}$  and band index  $s$ . For instance, in the particular Hamiltonian (3) the wave functions  $\Phi_{s,\mathbf{k}}(\mathbf{r})$  are given by Eq. (7). We define  $\mathcal{E}(s, \mathbf{k})$  to be the corresponding eigenvalue

$$H(\mathbf{p})\Phi_{s,\mathbf{k}}(\mathbf{r}) = \mathcal{E}(s, \mathbf{k})\Phi_{s,\mathbf{k}}(\mathbf{r}). \quad (13)$$

The time-periodic potential is given by

$$V(x, t) = \begin{cases} V_0 + V_1 \cos(\omega t), & \text{for } 0 < x < D, \\ 0, & \text{otherwise,} \end{cases} \quad (14)$$

which can be created through external metallic gates with a harmonically varying electric potential [14]. We divide the system in three regions, namely,  $x \leq 0$ ,  $0 \leq x \leq D$ , and  $D \leq x$ , denoted by regions I, II, and III respectively. We define

$$\alpha = \frac{V_1}{\hbar\omega} \quad (15)$$

and find the general plane wave solutions for all three regions:

$$W_{s_I k_I}(\mathbf{r}, t) = \Phi_{s_I, \mathbf{k}_I}(\mathbf{r}) \exp[-i\mathcal{E}(s_I, \mathbf{k}_I)t/\hbar], \quad (16a)$$

$$\begin{aligned} W_{s_{II} k_{II}}(\mathbf{r}, t) &= \Phi_{s_{II}, \mathbf{k}_{II}}(\mathbf{r}) \exp[-(i/\hbar)(V_0 t \\ &+ \mathcal{E}(s_{II}, \mathbf{k}_{II})t + V_1 \sin(\omega t)/\omega)] \\ &= \Phi_{s_{II}, \mathbf{k}_{II}}(\mathbf{r}) \sum_{m=-\infty}^{\infty} J_m(\alpha) \exp[-(i/\hbar)(V_0 \\ &+ \mathcal{E}(s_{II}, \mathbf{k}_{II}) + m\hbar\omega)t], \end{aligned} \quad (16b)$$

$$W_{s_{III} k_{III}}(\mathbf{r}, t) = \Phi_{s_{III}, \mathbf{k}_{III}}(\mathbf{r}) \exp[-i\mathcal{E}(s_{III}, \mathbf{k}_{III})t/\hbar]. \quad (16c)$$

The second equality in Eq. (16b) follows from the identity

$$\exp[-i\alpha \sin(\omega t)] = \sum_{m=-\infty}^{\infty} J_m(\alpha) e^{-im\omega t}, \quad (17)$$

where  $J_m(\alpha)$  are Bessel functions of the first kind. We now determine linear superpositions of these various solutions  $\Phi_{s_I, \mathbf{k}_I}(\mathbf{r}, t)$ ,  $\Phi_{s_{II}, \mathbf{k}_{II}}(\mathbf{r}, t)$ , and  $\Phi_{s_{III}, \mathbf{k}_{III}}(\mathbf{r}, t)$  in such a way as to yield continuous behavior at the interfaces  $x = 0$  and  $x = D$  for all times.

We assume that the incoming wave in region I is characterized by a wave vector  $\mathbf{k}_0$  and a band index  $s_0$ . To match this in region II, we need all momenta  $\mathbf{q}_m$  such that

$$E := \mathcal{E}(s_0, \mathbf{k}_0) = \mathcal{E}(s'_m, \mathbf{q}_m^\pm) + V_0 + m\hbar\omega, \quad (18a)$$

$$k_{y,0} = q_{y,m}^\pm, \quad (18b)$$

where the second relation follows from the conservation of  $k_{y,0}$  at all interfaces. The expressions (18a) are the sidebands for the system described by the Hamiltonian  $H(\mathbf{p})$  in the presence of the time-periodic potential  $V(x, t)$ . Using the specific Hamiltonian of uniaxially strained graphene (3) in this general development, we have

$$q_{m,x}^\pm = \pm s'_m \sqrt{\frac{(E - V_0 - m\hbar\omega)^2}{\hbar^2 v_x^2} - \frac{v_y^2}{v_x^2} k_{y,0}^2 \sin^2(\mu_x + \mu_y)} - k_{y,0} \tan \theta_{KT}, \quad (19a)$$

$$s'_m = \text{sgn}(E - V_0 - m\hbar\omega), \quad (19b)$$

where the  $\pm$  sign indicates the two possible solutions for  $q_m$ , which are obtained by the dispersion relation (11). There are two states with these wave vectors  $q_m$  and the same energy, we shall use them to represent “left-going” and “right-going” waves in region II, in the same way as it would happen with  $k_x$  and  $-k_x$  in isotropic systems. Now, to match the  $e^{-im\omega t}$  behavior in region II, we must introduce the wave vectors  $\mathbf{k}_m$  in regions I and III, defined by

$$\mathcal{E}(s_m, \mathbf{k}_m^\pm) = E - m\hbar\omega, \quad (20a)$$

$$k_{y,0} = k_{y,m}^\pm. \quad (20b)$$

Note again that  $\mathbf{k}_m^\pm$  are uniquely determined by  $\mathbf{k}_0$ . Also, the  $\pm$  sign is related to a choice of left-going and out-going waves, see Eq. (21a). Similarly, the solution of Eq. (20) is given by:

$$k_{x,m}^\pm = \pm s_m \sqrt{\frac{(E - m\hbar\omega)^2}{\hbar^2 v_x^2} - \frac{v_y^2}{v_x^2} k_{y,0}^2 \sin^2(\mu_x + \mu_y)} - k_{y,0} \tan \theta_{KT}, \quad (21a)$$

$$s_m = \text{sgn}(E - m\hbar\omega). \quad (21b)$$

It is possible to express  $k_{y,0}$  in terms of the incidence angle  $\theta$  inverting Eq. (9)

$$k_{y,0} = \frac{v_x |E| (\tan \theta - \tan \theta_{KT})}{\hbar v_y^2 \sin^2(\mu_x + \mu_y) \sqrt{1 + \frac{v_x^2 (\tan \theta - \tan \theta_{KT})^2}{v_y^2 \sin^2(\mu_x + \mu_y)}}}. \quad (22)$$

Using the above expression and the linear conservation of  $k_{y,0}$  in Eqs. (18b) and (20b), we can establish the generalized electron optics laws from Floquet scattering theory

$$\tan \theta_m^\pm = \frac{n_0^- (\tan \theta - \tan \theta_{KT})}{n_m^\pm \sqrt{1 + \left[1 - \left(\frac{n_0^-}{n_m^\pm}\right)^2\right] \left(\frac{v_x (\tan \theta - \tan \theta_{KT})}{v_y \sin(\mu_x + \mu_y)}\right)^2}} \pm \tan \theta_{KT}, \quad (23)$$

where  $\theta_m^-$  and  $\theta_m^+$  are the reflection and refraction angles for the sideband  $m$ . The effective refraction index is defined as

$$n_m^\pm = \frac{E - (1 \pm 1)V_0/2 - m\hbar\omega}{v_y \sin(\mu_x + \mu_y)}. \quad (24)$$

To identify the incidence range for propagating waves, we obtain the critical angles  $\theta_{c,m}^{d,\pm}$  in each sideband  $m$

$$\tan \theta_{c,m}^{d,\pm} = \tan \theta_{KT} + (-1)^d \frac{v_y \sin(\mu_x + \mu_y)}{v_x \sqrt{\left(\frac{n_0^-}{n_m^\pm}\right)^2 - 1}}, \quad (25)$$

where the index  $d = 1, 2$  corresponds to the minimum and maximum critical angle, respectively. It is important to note that there are critical angles for the reflection and refraction, which are indicated by the sign in the refraction index  $n_m^\pm$ .

We now make the following ansatz for the wave function  $\psi(\mathbf{r}, t)$  in terms of the band index and wave vector values in the three different regions I, II, and III:

$$\psi^I(\mathbf{r}, t) = \frac{1}{\sqrt{2}} e^{ik_y y} e^{-iEt/\hbar} \left[ \begin{aligned} & \left( \begin{array}{c} 1 \\ s_0 e^{i\phi_0^+} \end{array} \right) e^{ik_{x,0}^+ x} \\ & + \sum_{m=-\infty}^{\infty} r_m \left( \begin{array}{c} 1 \\ s_m e^{i\phi_m^-} \end{array} \right) e^{ik_{x,m}^- x} e^{-im\omega t} \end{aligned} \right], \quad (26a)$$

$$\psi^{II}(\mathbf{r}, t) = \frac{1}{\sqrt{2}} e^{ik_y y} e^{-iEt/\hbar} \sum_{n,m=-\infty}^{\infty} J_n(\alpha) \left[ \begin{aligned} & t'_m \left( \begin{array}{c} 1 \\ s'_m e^{i\phi_m^+} \end{array} \right) \\ & \times e^{iq_{x,m}^+ x} + r'_m \left( \begin{array}{c} 1 \\ s'_m e^{i\phi_m^-} \end{array} \right) e^{iq_{x,m}^- x} \end{aligned} \right] e^{-i(n+m)\omega t}, \quad (26b)$$

$$\psi^{III}(\mathbf{r}, t) = \frac{1}{\sqrt{2}} e^{ik_y y} e^{-iEt/\hbar} \sum_{m=-\infty}^{\infty} t_m \left( \begin{array}{c} 1 \\ s_m e^{i\phi_m^+} \end{array} \right) \times e^{ik_{x,m}^+ x} e^{-im\omega t}, \quad (26c)$$

where we define the phases corresponding to the various wave vectors, as described in Eq. (8)

$$\phi_m^\pm = \phi(\mathbf{k}_m^\pm), \quad (27)$$

$$\xi_m^\pm = \phi(\mathbf{q}_m^\pm), \quad (28)$$

and we use the particular eigenstates (7). The coefficient  $r_m$  is the reflection amplitude of the incident wave back into region I;  $t'_m$  and  $r'_m$  are the amplitudes of the right-going and left-going waves in region II respectively; and  $t_m$  is the total transmission amplitude from I to III, while gaining or losing an energy  $m\hbar\omega$  in the process. The sideband index indicates the conduction ( $s'_m = 1$ ) or valence ( $s'_m = -1$ ) band.

With the matching of the wave functions (26) at ( $x = 0$ ) and ( $x = D$ ) and using the orthonormality condition of Fourier basis, we obtain the following equations system:

$$\delta_{m0} + r_m = \sum_{l=-\infty}^{\infty} J_{m-l}(\alpha) (t'_l + r'_l), \quad (29a)$$

$$s_m \delta_{m0} e^{i\phi_m^+} + s_m r_m e^{i\phi_m^-} = \sum_{l=-\infty}^{\infty} s'_l J_{m-l}(\alpha) (t'_l e^{i\xi_l^+} + r'_l e^{i\xi_l^-}), \quad (29b)$$

$$t_m e^{ik_{x,m}^+ D} = \sum_{l=-\infty}^{\infty} J_{m-l}(\alpha) (t'_l e^{iq_{x,l}^+ D} + r'_l e^{iq_{x,l}^- D}), \quad (29c)$$

$$s_m t_m e^{ik_{x,m}^+ D} e^{i\phi_m^+} = \sum_{l=-\infty}^{\infty} s'_l J_{m-l}(\alpha) (t'_l e^{iq_{x,l}^+ D} e^{i\xi_l^+} + r'_l e^{iq_{x,l}^- D} e^{i\xi_l^-}), \quad (29d)$$

The linear equations system (29) must be truncated up to a maximum number of terms because, in principle, it is infinite. We can define this maximum number  $L$  in the sum and impose the conditions

$$r_m = t'_m = r'_m = t_m = 0, \quad (|m| \geq L + 1). \quad (30)$$

In this way, the dimension of the system is  $d \times d$ , where  $d = 4(2L + 1)$ , and the sum index  $m$  runs over  $-L$  to  $L$ . We chose the ordered basis for the amplitude coefficients defining the vector of  $d$  components by

$$\begin{aligned} \mathbf{X} &= (r_{-L}, \dots, r_L, t'_{-L}, \dots, t'_L, r'_{-L}, \dots, r'_L, t_{-L}, \dots, t_L)^T \\ &= [(r_m)_{m=-L}^L, (t'_m)_{m=-L}^L, (r'_m)_{m=-L}^L, (t_m)_{m=-L}^L]^T, \end{aligned} \quad (31)$$

where we use the notation  $(a_m)_{m=-L}^L = a_{-L}, \dots, a_L$  with  $a_m = r_m, t'_m, r'_m$  or  $t_m$ . We now write the equations system (29) in a slightly more compact form as follows:

$$\mathcal{M}_1 = [-\mathcal{I} \mathcal{J} \mathcal{J} \mathcal{O}], \quad (32a)$$

$$\mathcal{M}_2 = [\mathcal{O} \mathcal{J} \mathcal{J} - \mathcal{I}], \quad (32b)$$

$$\mathcal{J} = \mathcal{J}_{ml} = J_{m-l}(\alpha), \quad (32c)$$

$$\begin{aligned} \mathcal{D}_1 &= \text{diag}[(s_m e^{i\phi_m^-})_{m=-L}^L (s'_m e^{i\xi_m^+})_{m=-L}^L \\ &\quad (s'_m e^{i\xi_m^-})_{m=-L}^L (s_m e^{i\phi_m^+})_{m=-L}^L], \end{aligned} \quad (32d)$$

$$\begin{aligned} \mathcal{D}_2 &= \text{diag}[(e^{ik_{x,m}^- D})_{m=-L}^L (e^{iq_{x,m}^+ D})_{m=-L}^L \\ &\quad (e^{iq_{x,m}^- D})_{m=-L}^L (e^{ik_{x,m}^+ D})_{m=-L}^L], \end{aligned} \quad (32e)$$

$$\mathbf{b}_1 = (\delta_{m,0})_{m=-L}^L, \quad (32f)$$

$$\mathbf{b}_2 = s_0 e^{i\phi_0} \mathbf{b}_1, \quad (32g)$$

where the square submatrices  $\mathcal{I}$  and  $\mathcal{O}$  are the identity and null matrix of size  $d/4 \times d/4$ , respectively. Therefore, Eqs. (29) can be written as,

$$\mathcal{M}_1 \mathbf{X} = \mathbf{b}_1, \quad (33a)$$

$$\mathcal{M}_1 \mathcal{D}_1 \mathbf{X} = \mathbf{b}_2, \quad (33b)$$

$$\mathcal{M}_2 \mathcal{D}_2 \mathbf{X} = \mathbf{0}, \quad (33c)$$

$$\mathcal{M}_2 \mathcal{D}_1 \mathcal{D}_2 \mathbf{X} = \mathbf{0}. \quad (33d)$$

On the one hand, we can identify that the rectangular matrices  $\mathcal{M}_1$  and  $\mathcal{M}_2$  control the scattering of electrons in the time-periodic potential barrier through a unique tunable parameter  $\alpha$ . On the other hand, the diagonal matrices  $\mathcal{D}_1$  and  $\mathcal{D}_2$  contain the effect of strain from the phases in Eq. (27) and wave vectors given by Eqs. (19a) and (21a). The photon-assisted tunneling amplitudes  $t_m$  are provided by the last  $2L + 1$  components of vector

$$\mathbf{X} = \mathcal{M}^{-1} \mathbf{b}, \quad (34a)$$

$$\mathcal{M} = [\mathcal{M}_1 \quad \mathcal{M}_1 \mathcal{D}_1 \quad \mathcal{M}_2 \mathcal{D}_2 \quad \mathcal{M}_2 \mathcal{D}_1 \mathcal{D}_2]^T. \quad (34b)$$

Here  $\mathcal{M}$  is the total square matrix of the system defined by Eqs. (29a) to (29d) and  $\mathbf{b} = (\mathbf{b}_1, \mathbf{b}_2, \mathbf{0}, \mathbf{0})$ . Therefore, the

coefficients are given by  $T_m = |t_m|^2$  which quantify the transmission probabilities of electrons from the central band  $E$  to cross the time-periodic potential barrier and transit to the sideband  $E - m\hbar\omega$ .

In Appendix A, we show an approximate solution of this equation system with validity in the range  $0 < \alpha < 1$ .

#### IV. DISCUSSION AND RESULTS

The application of uniaxial strain along the  $\zeta = 45^\circ$  changes drastically the transport properties in anisotropic hexagonal materials. Electrons impinging the electrostatic potential barrier at the specific incidence angle  $\theta_{KT}$  present the anomalous Klein tunneling [107]. This effect emerges for strains that break the mirror symmetry with respect to the  $x$  axis. We set the values  $\epsilon = 10\%$  and  $\zeta = 45^\circ$ , where anomalous Klein tunneling appears for the incidence angle  $\theta_{KT} = -10.8^\circ$  in the static barrier  $\alpha = 0$ , [see Fig. 2(a)]. This perfect transmission occurs when the wave vector is perpendicular to the barrier, as obtained setting  $k_{y,0} = 0$  in Eq. (9). The incidence angle is different to zero due to that the wave vector, pseudospin, and group velocities are generally not parallel [31,107]. If we turn on the time-periodic potential, the anomalous Klein tunneling suppresses. The transmission probabilities in the central and sidebands depend on  $\alpha$ . In most of the cases, we only consider the transmission coefficients  $T_m$  with  $m = -2, -1, 0, 1, 2$  because the other ones with  $|m| > 2$  have a maximum value smaller than 0.1 in the whole range of  $0 < \alpha < 8$  and therefore they can be neglected. There are consistent numerical solutions of  $T_m$  with values  $L > 8$ . We chose  $L = 11$  which corresponds to solve numerically the linear equation system in Eq. (34a) of dimension  $92 \times 92$ . The transmission probability  $T_m$  starts to be relevant for  $\alpha > |m|$ , as shown in Fig. 2. We can see that electrons absorbing or emitting  $m$  photons have the same probability to cross the barrier [see Fig. 2(a)]. This equiprobability appears for the specific case where the wave vector is perpendicular to the barrier and also by the linear dispersion relation of electrons.

When electrons impinge under normal incidence to the time-periodic potential, as shown in Figs. 2(b) and 2(c), the wave vector is not perpendicular anymore as a consequence of the uniaxial strain out of the main axes  $x$  and  $y$ . This is contrary to the unstrained case, where it is perpendicular to the barrier and perfect transmission is observed for  $\alpha = 0$  [49,115]. Due to the strain the Dirac cones are elliptical and rotated in the low-energy regime, Klein tunneling deviates from the normal direction, and the transmission probability splits out slightly for the absorption and emission of photons, namely,  $T_m \neq T_{-m}$ . This splitting of the transmission probabilities has a different origin in comparison to isotropic and gapped graphene in time-periodic potentials [49,50,53]. The perfect transmission for normal incidence by the Klein tunneling in the static case  $\alpha = 0$  is destroyed, as verified by changing the energy values to  $E = 90$  and  $120$  meV in Figs. 2(b) and 2(c). This resonant tunneling is atypical for normal incidence. In a related system, the Hartman effect of a strained graphene barrier with a time-dependent oscillating potential has been studied [51]. However, in this setup a relative shift of the Dirac points occurs, which can be

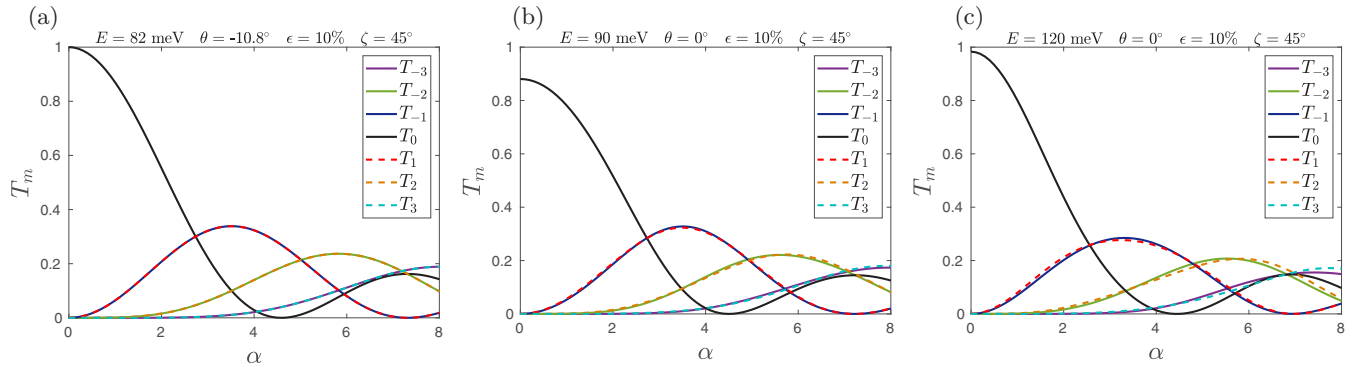


FIG. 2. Transmission probability  $T_m = |t_m|^2$  for electrons with energy  $E$  from the central band to cross the oscillating barrier and lie on the sideband  $E - m\hbar\omega$ . This transmission is obtained from the numerical solution of the linear equation system (34b), as a function of the ratio  $\alpha = V_1/\hbar\omega$ , where  $V_1$  is the oscillation amplitude for a time-periodic potential of height  $V_0 = 200$  meV, width  $D = 100$  nm, and frequency  $\omega = 5$  THz. The set of uniaxial strain parameters are  $\epsilon = 10\%$  and  $\zeta = 45^\circ$ . Transmission probability for the cases of anomalous Klein tunneling in the incidence angle  $\theta_{KT} = -10.8^\circ$  and using the energy  $E = 82$  meV in (a) normal incidence in (b), (c) for the energies  $E = 90$  and 120 meV, respectively.

misinterpreted as the opening of a band gap and lead to erroneous conclusions [51].

We call anomalous Floquet tunneling to the angular shift of the transmission maximum of the sidebands by the application of a uniaxial tension different to the direction  $\zeta = 0^\circ$  and  $90^\circ$ , as shown in Figs. 3(a) to 3(f). For isotropic systems, the angular shift in the transmission probability appears by time-reversal symmetry breaking with an external magnetic field [66]. The vector potential, which generates the magnetic field, shifts the Dirac cone in the reciprocal space. In the present work, the strain affects the Dirac cone differently changing

the circular shape to a rotated and elliptical one. The common feature here with systems presenting time-reversal symmetry breaking is due to that incident electrons with a wave vector perpendicular to the interface have a nonzero parallel group velocity  $v_y$ . In Fig. 3, we chose a shortened incidence angle range to avoid the evanescent waves. The incident electrons have critical angles that depend on the sideband, which are given by the expressions in Eq. (25). Increasing  $\epsilon$  in Figs. 3(a) to 3(c), we observe that this angular deviation in the maximum of transmissions improves. Moreover, we can see in Figs. 3(d) to 3(f) that the tensile strain also affects the transmission

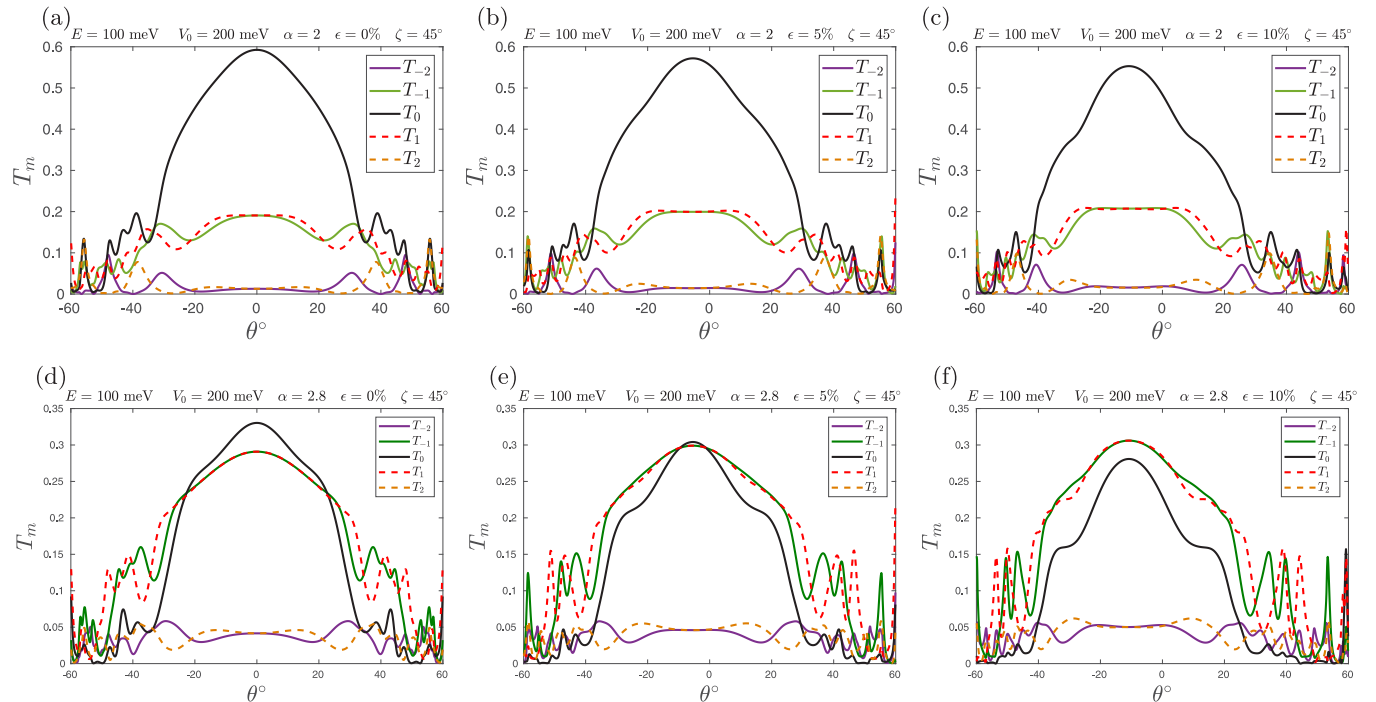


FIG. 3. Anomalous Floquet tunneling of electrons at the energy  $E = 100$  meV as a function of the incidence angle  $\theta$ . The set of values for the time-periodic potential are  $V_0 = 200$  meV,  $D = 100$  nm, and  $\omega = 5$  THz. Transmission probabilities  $T_m = |t_m|^2$  using the strain parameters  $\epsilon = 0, 5, 10\%$  and  $\zeta = 45^\circ$  with  $\alpha = 2$  in (a), (b), and (c), and  $\alpha = 2.8$  in (d), (e), and (f), respectively.

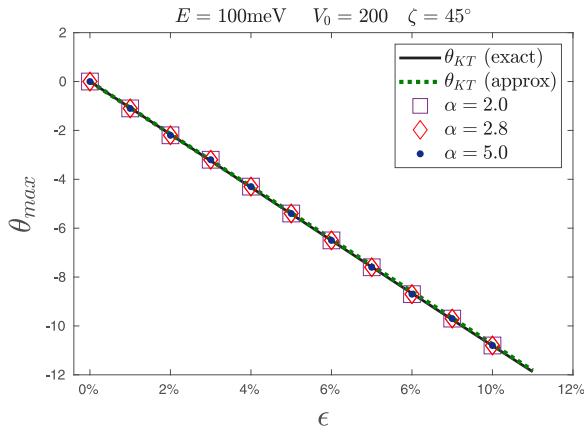


FIG. 4. Anomalous Klein tunneling angle [Eqs. (10) and (35)] and the numerically determined angular shift of the transmission maximum  $T_0$ ,  $T_1$ , and  $T_{-1}$  as a function of the tensile strain parameter  $\epsilon$  at the direction  $\zeta = 45^\circ$  and the ratio  $\alpha = V_1/\hbar\omega = 2, 2.8$ , and  $5$ .

maximum of the sidebands. The value of  $T_0$  for normal incidence is bigger than the other transmissions  $T_m$  when  $\epsilon = 0$ , but increasing the tensile strain, the maximum of  $T_0$  decreases being now less than the ones of  $T_1$  and  $T_{-1}$ . Hence, the uniaxial strain is useful to favor the transmission of inelastic tunneling and generate photoinduced electronic currents.

We show in Fig. 4 the angular shift of the transmission maximum  $\theta_{max}$  as a function of the tensile strain. This angular shift has a good agreement with the anomalous Klein tunneling angle  $\theta_{KT}$  predicted by Eq. (10). It is worth noting that this angular shift of the transmission maximum depends only on the tensile strain  $\epsilon$  and tension angle  $\zeta$ . We find that  $\theta_m$  for all values of  $\alpha$  follows the linear behavior of  $\theta_{KT}$ . This indicates that the conservation of pseudospin in this direction is persistent and robust enough, being unaffected by the time-periodic potential barrier. The expansion of Eq. (10) (see Appendix B), keeping only the first-order terms in  $\epsilon$ , we lead to a very simple and straightforward relation of the anomalous Klein tunneling angle with the parameters  $\epsilon$  and  $\zeta$

$$\theta_{KT} \approx \frac{360^\circ}{\pi} \rho^+ (1 - \beta) \epsilon \sin 2\zeta, \quad (35)$$

which has a negligible deviation of the exact relation (10) in the whole strain range considered. It is important to note that  $\theta_{KT}$  indicates the direction for the conservation of the pseudospin. For this reason, the anomalous Klein tunneling, though largely suppressed, can be recognized in Fig. 3. Uniaxial strain along with the directions  $\zeta = 0^\circ$  and  $90^\circ$  (not shown) does not break the mirror symmetry with respect to the normal axis. In this case, the group velocity and the wave vector are parallel for normal incidence which restores the angular transmission symmetry. We quantify the anomaly in the transmissions using the direction of the Klein tunneling deviation in Eq. (10), which depends only on the strain parameters  $\epsilon$  and  $\zeta$ . Figure 5 shows this anomaly in the whole strain range. As expected, the uniaxial strains along the perpendicular and parallel directions to the interface keep the symmetry in the transmission. While tensions in a different direction to  $\zeta \neq 0$  and  $90^\circ$  cause the anomalous Floquet tunneling. We find that

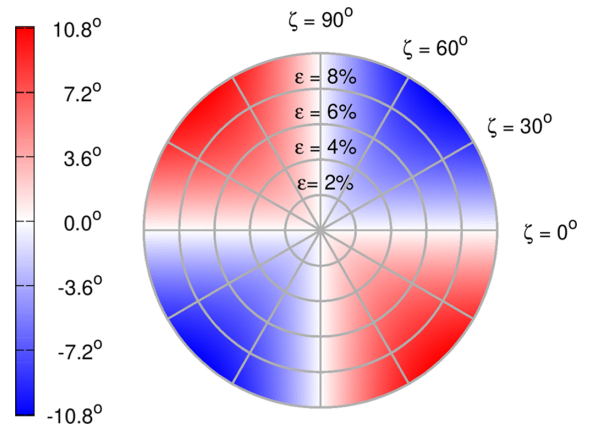


FIG. 5. Anomalous Klein tunneling angle as a function of the strain parameters  $\epsilon$  (radius from 0 to 10%) and  $\zeta$  (polar angle in degrees).

the highest angular shift value is  $\theta_{KT} \approx -10.8^\circ$  for the set of parameters  $\epsilon = 10\%$  and  $\zeta = 45^\circ$ .

We show in Fig. 6 the Floquet scattering angles of electron beams impinging the interface of time-periodic barriers. We can see that the reflected and refracted beams depend on the sideband energy. The inelastic electron scattering process changes the direction of the propagation wave with probabilities determined by the amplitudes  $r_m$  and  $t_m$ . This behavior is similar to Compton scattering, where the photon changes its direction and energy by the collision with the electron. However, the electron interacts absorbing or emitting a photon of energy  $m\hbar\omega$ , and the anisotropy induced by the tensile strain leads to generalized Snell's laws, as shown in Fig. 6. The application of uniaxial strain out to the axes  $x$  and  $y$

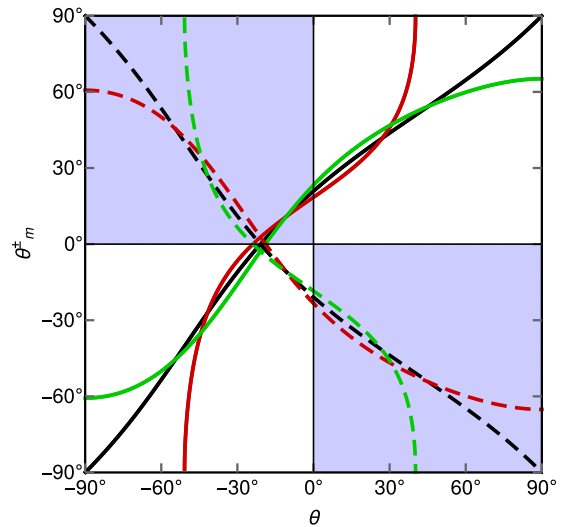


FIG. 6. Electron optics laws from Floquet scattering theory. The solid (dashed) curves correspond to reflection (refraction) angles as a function of the incidence angle for the central band (black) and the sidebands  $m = -2$  (green) and  $m = 2$  (red), using Eqs. (23) with the set of values  $E = 25$  meV,  $V_0 = 50$  meV,  $\epsilon = 10\%$ ,  $\zeta = 45^\circ$ , and  $\omega = 5$  THz. The blue (white) region indicates negative (positive) reflection and refraction.

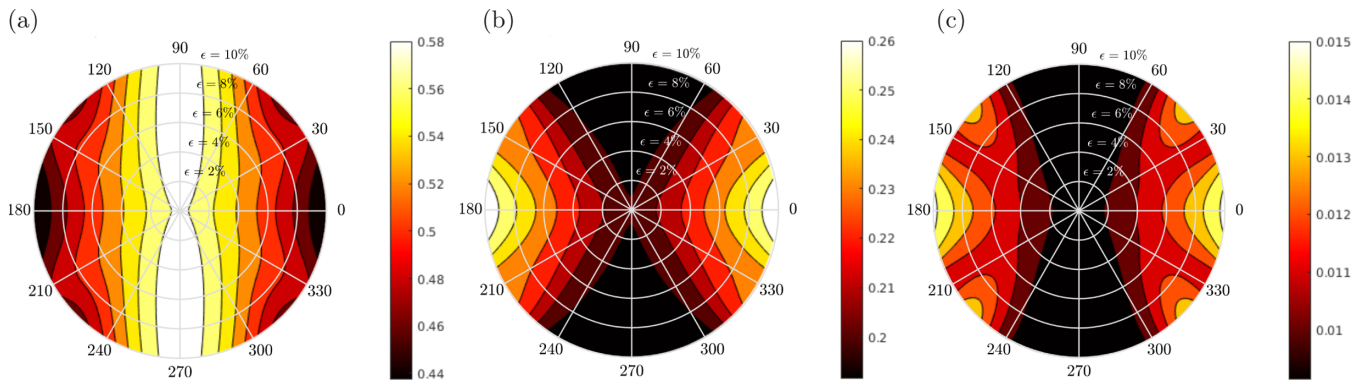


FIG. 7. Transmission probability (a)  $T_0$ , (b)  $T_{-1}$ , and (c)  $T_{-2}$  as a function of uniaxial strain parameters  $\epsilon$  (radius from 0 to 10%) and  $\zeta$  (polar angle in degrees) for electrons with normal incidence and energy  $E = 100$  meV in a time-periodic potential  $V_0 = 200$  meV,  $D = 100$  nm,  $\alpha = 2$ , and  $\omega = 5$  THz.

causes negative reflection for the electrons in the sidebands with an incidence angle in the range from  $-30^\circ$  to  $0^\circ$ . We can also observe partial positive refraction of electrons in the same incidence range. It is important to note that there are critical angles for the reflection, as predicted by Eqs. (25), and they are due to photon emission processes. In a symmetric barrier  $V_0 = 2E$ , these critical angles for the refraction are identical to the reflection ones in the absorption of photons. Such electron scattering phenomena are summarized in the optics laws Eqs. (23), where the refraction index media is determined by the uniaxial strain and sideband energies.

To understand how the uniaxial strain affects the behavior of photon-assisted tunneling, we show the probability transmission as a function of  $\epsilon$  and  $\zeta$  in Fig. 7 for the case of normal incidence. We can see that in a wide range of  $\zeta$ , the behavior of  $T_m$  is strongly anisotropic with the angle  $\zeta$ , and the increase of  $\epsilon$  causes a reduction in the probability transmission  $T_0$ , as shown in Fig. 7(a). However, for the tension angle  $\zeta = 90^\circ$ , normal incident electrons have an almost constant probability of crossing the barrier regardless of the tensile strain. It is worth noting that the independence of transmission on the tensile strain at  $\zeta = 90^\circ$  also appears for other sidebands, as shown in Figs. 7(b) and 7(c). The transmission  $T_1$  and  $T_2$  present an identical behavior with respect to the emission counterpart. The application of strain in the directions near the  $x$ -axis shows an increase of  $T_{-1}$  and  $T_{-2}$ . While uniaxial strain

along the  $y$ -axis decreases the electron transmission in the sidebands. The time exposition of electrons to the oscillating barrier explains the strain-induced transition from elastic to inelastic tunneling. Positive tensile strains in the direction  $\zeta = 0^\circ$  increase the bond lengths. Therefore, the probability amplitude of electrons decreases to hop among neighboring sites. In this way, there is more time exposition to interact with the time-periodic potential. Thus, electrons cross the barrier inelastically with transmission probabilities  $T_1$  and  $T_2$ . In contrast, deformations parallel to the interface decrease the zigzag bond lengths, and electrons have a major probability to cross the barrier elastically.

We examine the behavior of the transmission probability  $T_m$  as a function of barrier width and incidence angle, as shown in Fig. 8. In general, the reminiscence of the anomalous Klein tunneling makes that almost all the transmission occurs around the incident angle  $\theta = -10.8^\circ$ . We find that the tuning of barrier width can serve as a selector of the transmission in the sidebands. In thin barriers  $D < 50$  nm [see Fig. 8(a)], the transmission is mainly due to the central band, where other sidebands participate only scarcely. The increase of the barrier width can suppress the transmission in the central band and favors the emergence of another transmissions in the sidebands. Figure 8(b) shows that electrons absorbing or emitting one photon have a higher probability of crossing the time-periodic barrier if the width is within the range of 100 to 150 nm. The

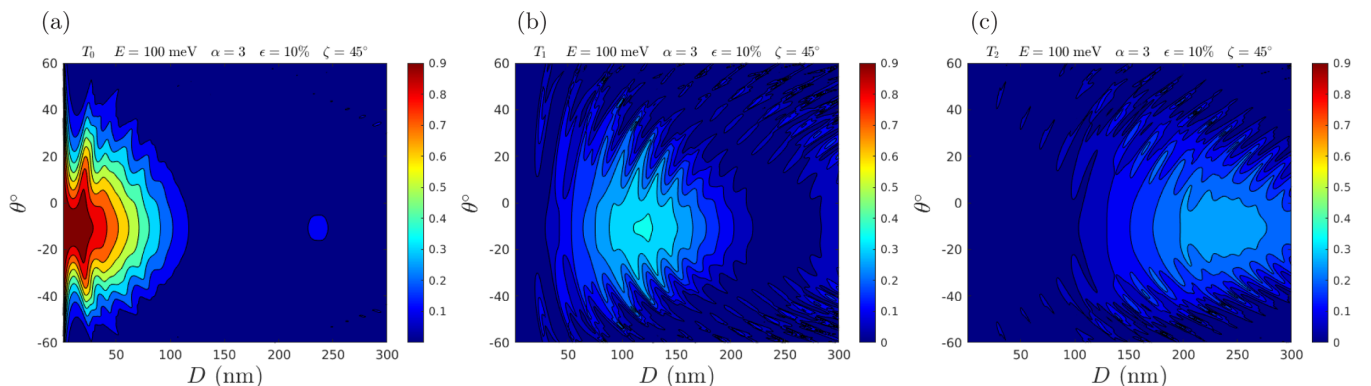


FIG. 8. Transmission probabilities of (a)  $T_0$ , (b)  $T_1$ , and (c)  $T_2$  as a function of barrier width and incidence angle for the potential height  $V_0 = 200$  meV.



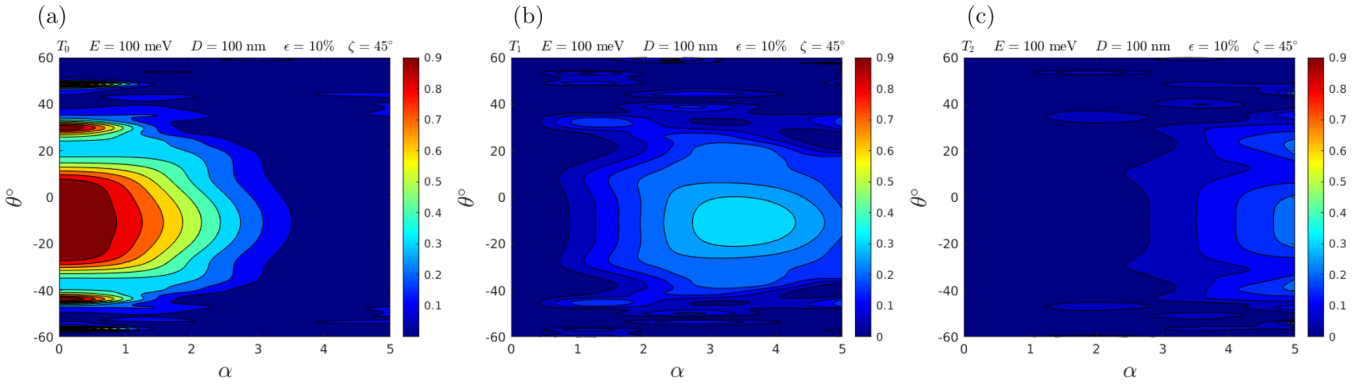


FIG. 9. Transmission probabilities of (a)  $T_0$ , (b)  $T_1$ , and (c)  $T_2$  as a function of the parameter  $\alpha$  and incidence angle  $\theta$  for the potential height  $V_0 = 200$  meV and width  $D = 100$  nm.

same occurs for  $T_2$  in Fig. 8(c) in the range  $150 < D < 300$  nm. This is due to the fact that, for electrons to cross the barrier, they need more exposition time to interact with the time-periodic potential, and therefore, it favors the promotion of electrons to travel through other sidebands with a higher energy difference. We note a similar behavior (not shown) for the transmissions  $T_{-1}$  and  $T_{-2}$  compared with  $T_1$  and  $T_2$ , respectively. These results imply that an adequate selection of the barrier width allows that the device converts incoming electron current with energy  $E$  to two outgoing photoexcited currents, with a difference between them of  $2n\hbar\omega$ . The uniaxial deformation improves the inelastic tunneling and enhances the output of photon-excited currents (in comparison to isotropic systems [19–21]).

Another alternative way to select transmission in a particular sideband is to modulate the oscillating amplitude  $V_1$ . Figure 9 shows the transmissions  $T_0$ ,  $T_1$ , and  $T_2$  as a function of  $\alpha$  and  $\theta$  for a constant value of the barrier width. Anomalous Klein tunneling and resonant peaks are suppressed by increasing  $\alpha$ , while electron transmissions in other sidebands arise. Dependent on the amplitude of the oscillation, the device in Fig. 1(a), can convert electron current to a photoexcited one.

## V. CONCLUSION AND FINAL REMARKS

We study the effect of uniaxial strain on the transport properties of electrons in graphene in the presence of a photon-assisted tunneling mechanics. The interplay of uniaxial strain and photon-assisted tunneling opens possibilities to control electron flow. We applied the Floquet scattering theory in anisotropic hexagonal lattices. This approach serves to understand the interaction of electron current with the

time-periodic potential in systems such as uniaxially strained graphene, photonic crystals, molecular graphene, and optical lattices. We calculate the transmission probabilities with the absorption or emission of multiphoton processes as well as the electron optics laws for time-periodic potentials. The main transmission features as anomalous Floquet tunneling and the modulation of the transmission maximum in the sidebands occur with the application of uniaxial strains out of the  $x$  and  $y$  axes. We find that applying uniaxial strain in the parallel direction at the interface, photon-assisted tunneling is unaffected by the increase of the tensile parameter. Whereas, uniaxial strain perpendicular to the barrier enhances the electron transmission from the sidebands. The generalized Snell's laws describes the scattering of electrons in the oscillating barrier, identifying negative reflection and positive refraction for interband tunneling, which depends on the sideband energies. An appropriate design of the barrier width, or tuning the amplitude of oscillation, can select the electron tunneling to absorb or emit  $n$  photons. Therefore, the device converts an electron current to a photoexcited one. Such findings may be useful to control the electron flow in nanoelectronic devices through the photon-assisted tunneling and strain engineering.

## ACKNOWLEDGMENTS

P.M. gratefully acknowledges a fellowship from UNAM-DGAPA. We acknowledge financial support from CONACYT Project A1-S-13469, CONACYT Project 254515, CONACYT Project Fronteras 952, and the UNAM-PAPIIT research Grants No. IA-103020 and No. IN113620. We thank T. H. Seligman and L. E. F. Foa-Torres for useful discussions and comments.

## APPENDIX A: APPROXIMATE SOLUTION OF FLOQUET SCATTERING OF ELECTRONS IN UNIAXIALLY STRAINED GRAPHENE

It is possible to obtain an approximate solution for the transmission coefficient  $T_j = |t_j|^2$  with  $j = -1$  and  $1$  using the exposed method in Sec. III. As we can see, the fact that the  $J_n(\alpha)$  is negligible at  $n \gg L$  in the range  $0 < \alpha < L$ , it causes that the infinite system evolves a finite one from  $-L$  up to  $L$ . In the case  $L = 0$ , the equation system has dimension  $d = 4$  and we can calculate the transmission coefficient for the static barrier

$$T_{sm} = \frac{\cos^2 \chi_m \cos^2 \chi'_m}{\cos^2 \chi_m \cos^2 \chi'_m \cos^2 \gamma'_m + [1 - s_m s'_m \sin \chi_m \sin \chi'_m]^2 \sin^2 \gamma'_m}, \quad (\text{A1})$$

which is the probability of an electron to cross the barrier from the same sideband with energy  $E - m\hbar\omega$ , where

$$\chi_m = \phi_m^+ + \mu_x, \quad (\text{A2a})$$

$$\chi'_m = \xi_m^+ + \mu_x, \quad (\text{A2b})$$

$$\gamma'_m = \frac{D|E - V_0 - m\hbar\omega|}{v_x\hbar} \cos(\xi_m^+ + \mu_x). \quad (\text{A2c})$$

Due to the dependence on barrier width in Eq. (A1), resonant tunneling occurs for  $\gamma'_m = N\pi$  being  $N$  an integer. While anomalous Klein tunneling appears for the incidence angle  $\theta = \theta_{KT}$ . Without deformation, the above values are  $\mu_x = 0$ ,  $\mu_y = \pi/2$ ,  $v_x = v_y = 1$ , recovering the expression of transmission coefficient in a static barrier of graphene [115]. With the definition of transmission probability in photon-assisted tunneling  $T_m = |t_m|^2$  and solving the equation systems for  $L = 1$ , we find an analytical transmission for the transmission  $T_1$  valid in the range  $0 < \alpha < 1$

$$T_1 = \left( \frac{J_1(\alpha)|(\Gamma_1 - \Gamma_0) + (\Lambda_1 - \Lambda_0)|}{J_0(\alpha)|e^{i\phi_1^+} - e^{i\phi_1^-}|} \right)^2 T_{s0}T_{s1}, \quad (\text{A3})$$

where the quantities  $\Gamma_j$  and  $\Lambda_j$  are defined as

$$\Gamma_j = \frac{e^{iq_{x,j}D}(e^{i\phi_1^-} + e^{i\xi_j^-})(e^{i\phi_0^+} + e^{i\xi_j^+})}{e^{i\xi_j^-} - e^{i\xi_j^+}}, \quad (\text{A4a})$$

$$\Lambda_j = \frac{e^{iq_{x,j}D}(e^{i\xi_j^+} + e^{i\phi_1^-})(e^{i\phi_0^+} + e^{i\xi_j^-})}{e^{i\xi_j^-} - e^{i\xi_j^+}}, \quad (\text{A4b})$$

with the index  $j = 0$  or  $1$ . An identical expression is obtained for the transmission  $T_{-1}$  replacing  $1 \rightarrow -1$  in all the relations above. In the unstrained case, the transmission probability (A3) is identical to those calculated in [49].

## APPENDIX B: LINEAR RELATION OF ANOMALOUS KLEIN TUNNELING ANGLE WITH THE UNIAXIAL STRAIN

To obtain the linear dependence on the tensile strain  $\epsilon$  of anomalous Klein tunneling angle, we expand Eq. (10) keeping the first-order in  $\epsilon$ . First, we calculate the ratio of the complex velocities components (4)

$$\frac{v_y^c}{v_x^c} = \frac{a_{1y}\tau_1 e^{-i\mathbf{K}_D \cdot \delta_1} + a_{2y}\tau_2 e^{-i\mathbf{K}_D \cdot \delta_2}}{a_{1x}\tau_1 e^{-i\mathbf{K}_D \cdot \delta_1} + a_{2x}\tau_2 e^{-i\mathbf{K}_D \cdot \delta_2}}. \quad (\text{B1})$$

This expression is useful to express Eq. (10) as

$$\theta_{KT} \approx \frac{180^\circ}{\pi} \text{Re}(v_y^c/v_x^c) = \frac{180^\circ}{\pi} \frac{a_{1x}a_{1y}\tau_1^2 + a_{2x}a_{2y}\tau_2^2 + (a_{1x}a_{2y} + a_{2x}a_{1y})\tau_1\tau_2 \cos[\mathbf{K}_D \cdot (\delta_1 - \delta_2)]}{a_{1x}^2\tau_1^2 + a_{2x}^2\tau_2^2 + 2a_{1x}a_{2x}\tau_1\tau_2 \cos[\mathbf{K}_D \cdot (\delta_1 - \delta_2)]}. \quad (\text{B2})$$

Taking into account that the solution for Eq. (5) is

$$\cos[\mathbf{K}_D \cdot (\delta_1 - \delta_2)] = \frac{\tau_3^2 - \tau_2^2 - \tau_1^2}{2\tau_1\tau_2} \quad (\text{B3})$$

and the deformed lengths of uniaxially strained graphene are

$$\delta_j \approx a\{1 + \rho^-\epsilon + \rho^+\epsilon \cos[2\zeta + (2j - 1)60^\circ]\}, \quad (\text{B4})$$

we expand the exponential decay rule for the hopping parameters  $\tau_j$  up to first order in  $\epsilon$

$$\frac{\tau_j}{\tau} \approx 1 - \beta\{\rho^- + \rho^+ \cos[2\zeta + (2j - 1)60^\circ]\}\epsilon. \quad (\text{B5})$$

Substituting the above expression in Eq. (B3)

$$\cos[\mathbf{K}_D \cdot (\delta_1 - \delta_2)] \approx -\frac{1}{2}[1 + 3\beta\rho^+\epsilon \cos(2\zeta - 60^\circ)]. \quad (\text{B6})$$

In the same way, we expand the relations

$$a_{1x}\tau_1 \approx \sqrt{3}a\tau(1 + c_{1x}\epsilon), \quad (\text{B7})$$

$$a_{1y}\tau_1 \approx \sqrt{3}a\tau\rho^+\epsilon \sin 2\zeta, \quad (\text{B8})$$

$$a_{2x}\tau_2 \approx \frac{\sqrt{3}}{2}a\tau(1 + c_{2x}\epsilon), \quad (\text{B9})$$

$$a_{2y}\tau_2 \approx \frac{\sqrt{3}}{2}a\tau(\sqrt{3} + c_{2y}\epsilon), \quad (\text{B10})$$

where we used Eqs. (1) and (B5). The coefficients  $c_{1x}$ ,  $c_{2x}$ , and  $c_{2y}$  are, respectively,

$$c_{1x} = \rho^- + \rho^+ \cos 2\zeta - \beta[\rho^- + \rho^+ \cos(2\zeta + 60^\circ)], \quad (\text{B11})$$

$$c_{2x} = \rho^- + 2\rho^+ \cos(2\zeta - 60^\circ) - \beta[\rho^- - \rho^+ \cos 2\zeta], \quad (\text{B12})$$

$$c_{2y} = \sqrt{3}\rho^- + 2\rho^+ \sin(2\zeta - 60^\circ) - \sqrt{3}\beta[\rho^- - \rho^+ \cos 2\zeta]. \quad (\text{B13})$$

Substituting the relations (B7) to (B10) and (B6) in Eq. (B2), we obtain

$$\begin{aligned} \theta_{KT} &\approx \frac{180^\circ}{\pi} \frac{2\rho^+(1-\beta)\epsilon \sin 2\zeta}{1 + 3[c_{1x} + c_{2x} - \beta\rho^+ \cos(2\zeta - 60^\circ)]\epsilon} \\ &\approx \frac{360^\circ}{\pi} \rho^+(1-\beta)\epsilon \sin 2\zeta, \end{aligned} \quad (\text{B14})$$

which is the result as shown in Eq. (35).

- 
- [1] A. H. Dayem and R. J. Martin, Quantum Interaction of Microwave Radiation with Tunneling Between Superconductors, *Phys. Rev. Lett.* **8**, 246 (1962).
- [2] T. E. Hartman, Tunneling of a wave packet, *J. Appl. Phys.* **33**, 3427 (1962).
- [3] P. K. Tien and J. P. Gordon, Multiphoton process observed in the interaction of microwave fields with the tunneling between superconductor films, *Phys. Rev.* **129**, 647 (1963).
- [4] J. H. Shirley, Solution of the Schrödinger equation with a Hamiltonian periodic in time, *Phys. Rev.* **138**, B979 (1965).
- [5] M. Büttiker and R. Landauer, Traversal Time for Tunneling, *Phys. Rev. Lett.* **49**, 1739 (1982).
- [6] J. R. Fletcher, Time delay in tunnelling through a potential barrier, *J. Phys. C: Solid State Phys.* **18**, L55 (1985).
- [7] F. Grossmann, T. Dittrich, P. Jung, and P. Hänggi, Coherent Destruction of Tunneling, *Phys. Rev. Lett.* **67**, 516 (1991).
- [8] M. Wagner, Quenching of resonant transmission through an oscillating quantum well, *Phys. Rev. B* **49**, 16544 (1994).
- [9] L. P. Kouwenhoven, S. Jauhar, J. Orenstein, P. L. McEuen, Y. Nagamune, J. Motohisa, and H. Sakaki, Observation of Photon-Assisted Tunneling through a Quantum Dot, *Phys. Rev. Lett.* **73**, 3443 (1994).
- [10] M. Wagner, Photon-assisted transmission through an oscillating quantum well: A transfer-matrix approach to coherent destruction of tunneling, *Phys. Rev. A* **51**, 798 (1995).
- [11] R. H. Blick, R. J. Haug, D. W. van der Weide, K. von Klitzing, and K. Eberl, Photon-assisted tunneling through a quantum dot at high microwave frequencies, *Appl. Phys. Lett.* **67**, 3924 (1995).
- [12] M. Wagner, Strongly Driven Quantum Wells: An Analytical Solution to the Time-Dependent Schrödinger Equation, *Phys. Rev. Lett.* **76**, 4010 (1996).
- [13] M. Wagner and W. Zwerger, Characteristic scaling parameters for tunneling in strong time-dependent electric fields, *Phys. Rev. B* **55**, R10217 (1997).
- [14] G. Platero and R. Aguado, Photon-assisted transport in semiconductor nanostructures, *Phys. Rep.* **395**, 1 (2004).
- [15] C.-X. Zhang, Y.-H. Nie, and J.-Q. Liang, Photon-assisted electron transmission resonance through a quantum well with spin-orbit coupling, *Phys. Rev. B* **73**, 085307 (2006).
- [16] B. Trauzettel, Y. M. Blanter, and A. F. Morpurgo, Photon-assisted electron transport in graphene: Scattering theory analysis, *Phys. Rev. B* **75**, 035305 (2007).
- [17] J. W. Schwede, I. Bargatin, D. C. Riley, B. E. Hardin, S. J. Rosenthal, Y. Sun, F. Schmitt, P. Pianetta, R. T. Howe, Z.-X. Shen, and N. A. Melosh, Photon-enhanced thermionic emission for solar concentrator systems, *Nat. Mater.* **9**, 762 (2010).
- [18] T. Mueller, F. Xia, and P. Avouris, Graphene photodetectors for high-speed optical communications, *Nat. Photonics* **4**, 297 (2010).
- [19] M. Freitag, T. Low, F. Xia, and P. Avouris, Photoconductivity of biased graphene, *Nat. Photonics* **7**, 53 (2012).
- [20] K. J. Tielrooij, J. C. W. Song, S. A. Jensen, A. Centeno, A. Pesquera, A. Z. Elorza, M. Bonn, L. S. Levitov, and F. H. L. Koppens, Photoexcitation cascade and multiple hot-carrier generation in graphene, *Nat. Phys.* **9**, 248 (2013).
- [21] Q. Ma, C. H. Lui, J. C. W. Song, Y. Lin, J. F. Kong, Y. Cao, T. H. Dinh, N. L. Nair, W. Fang, K. Watanabe, T. Taniguchi, S.-Y. Xu, J. Kong, T. Palacios, N. Gedik, N. M. Gabor, and P. Jarillo-Herrero, Giant intrinsic photoresponse in pristine graphene, *Nat. Nanotechnol.* **14**, 145 (2018).
- [22] V. Gudmundsson, O. Jonasson, C.-S. Tang, H.-S. Goan, and A. Manolescu, Time-dependent transport of electrons through a photon cavity, *Phys. Rev. B* **85**, 075306 (2012).
- [23] R. Biswas and C. Sinha, Photon induced tunneling of electron through a graphene electrostatic barrier, *J. Appl. Phys.* **114**, 183706 (2013).
- [24] A. Soltani, F. Kuschewski, M. Bonmann, A. Generalov, A. Vorobiev, F. Ludwig, M. M. Wiecha, D. Čibiraitė, F. Walla, S. Winnerl, S. C. Kehr, L. M. Eng, J. Stake, and H. G. Roskos, Direct nanoscopic observation of plasma waves in the channel of a graphene field-effect transistor, *Light Sci. Appl.* **9**, 97 (2020).
- [25] A. H. Castro Neto, F. Guinea, N. M. R. Peres, K. S. Novoselov, and A. K. Geim, The electronic properties of graphene, *Rev. Mod. Phys.* **81**, 109 (2009).
- [26] P. Vogt, P. DePadova, C. Quaresima, J. Avila, E. Frantzeskakis, M. C. Asensio, A. Resta, B. Ealet, and G. Le Lay, Silicene: Compelling Experimental Evidence for Graphenelike Two-Dimensional Silicon, *Phys. Rev. Lett.* **108**, 155501 (2012).

- [27] L. Li, S. Zan Lu, J. Pan, Z. Qin, Y. Qi Wang, Y. Wang, G. Yu Cao, S. Du, and H.-J. Gao, Buckled germanene formation on Pt(111), *Adv. Mater.* **26**, 4820 (2014).
- [28] T. Wehling, A. Black-Schaffer, and A. Balatsky, Dirac materials, *Adv. Phys.* **63**, 1 (2014).
- [29] A. Carvalho, M. Wang, X. Zhu, A. S. Rodin, H. Su, and A. H. C. Neto, Phosphorene: from theory to applications, *Nat. Rev. Mater.* **1**, 16061 (2016).
- [30] W. Li, L. Kong, C. Chen, J. Gou, S. Sheng, W. Zhang, H. Li, L. Chen, P. Cheng, and K. Wu, Experimental realization of honeycomb borophene, *Science Bulletin* **63**, 282 (2018).
- [31] Y. Betancur-Ocampo, F. Leyvraz, and T. Stegmann, Electron optics in phosphorene pn junctions: Negative reflection and anti-super-Klein tunneling, *Nano Lett.* **19**, 7760 (2019).
- [32] Y. Betancur-Ocampo, E. Paredes-Rocha, and T. Stegmann, Phosphorene pnp junctions as perfect electron waveguides, *J. Appl. Phys.* **128**, 114303 (2020).
- [33] R. Biswas, R. Dey, and C. Sinha, Transmission and conductance for a driven vector barrier in phosphorene, *Superlattices Microstruct.* **133**, 106175 (2019).
- [34] E. Díaz-Bautista and Y. Betancur-Ocampo, Phase-space representation of Landau and electron coherent states for uniaxially strained graphene, *Phys. Rev. B* **101**, 125402 (2020).
- [35] M. R. Setare, P. Majari, C. Noh, and S. Dehdashti, Photonic realization of the deformed Dirac equation via the segmented graphene nanoribbons under inhomogeneous strain, *J. Mod. Opt.* **66**, 1663 (2019).
- [36] E. Díaz-Bautista, Y. Concha-Sánchez, and A. Raya, Barut-Girardello coherent states for anisotropic 2D-Dirac materials, *J. Phys.: Condens. Matter* **31**, 435702 (2019).
- [37] L. Dell'Anna, P. Majari, and M. R. Setare, From Klein to anti-Klein tunneling in graphene tuning the Rashba spin-orbit interaction or the bilayer coupling, *J. Phys.: Condens. Matter* **30**, 415301 (2018).
- [38] P. Majari, A. Luis, and M. R. Setare, Mapping of the  $2 + 1$  q-deformed Dirac oscillator onto the q-deformed Jaynes-Cummings model, *Europhys. Lett.* **120**, 44002 (2017).
- [39] M. Yang, Q.-T. Hou, and R.-Q. Wang, Electronic non-coplanar refraction and deflected diffraction of Weyl-node-mismatch junctions, *New J. Phys.* **21**, 113057 (2019).
- [40] Y. Ren, Y. Gao, P. Wan, Q. Wang, D. Huang, and J. Du, Effective medium theory for electron waves in a gate-defined quantum dot array in graphene, *Phys. Rev. B* **100**, 045422 (2019).
- [41] P. Ghosh and P. Roy, Collapse of Landau levels in graphene under uniaxial strain, *Mater. Res. Express* **6**, 125603 (2019).
- [42] D.-N. Le, V.-H. Le, and P. Roy, Graphene under uniaxial inhomogeneous strain and an external electric field: Landau levels, electronic, magnetic and optical properties, *Eur. Phys. J. B* **93**, 158 (2020).
- [43] W. Li and L. E. Reichl, Floquet scattering through a time-periodic potential, *Phys. Rev. B* **60**, 15732 (1999).
- [44] M. Moskalets and M. Büttiker, Floquet scattering theory of quantum pumps, *Phys. Rev. B* **66**, 205320 (2002).
- [45] Z. Gu, H. A. Fertig, D. P. Arovas, and A. Auerbach, Floquet Spectrum and Transport through an Irradiated Graphene Ribbon, *Phys. Rev. Lett.* **107**, 216601 (2011).
- [46] T. Bilitewski and N. R. Cooper, Scattering theory for Floquet-Bloch states, *Phys. Rev. A* **91**, 033601 (2015).
- [47] S. E. Savel'ev and A. S. Alexandrov, Massless Dirac fermions in a laser field as a counterpart of graphene superlattices, *Phys. Rev. B* **84**, 035428 (2011).
- [48] C. Wurl and H. Fehske, Time-periodic Klein tunneling through optomechanical Dirac barriers, *Eur. Phys. J. Spec. Top.* **227**, 1995 (2019).
- [49] M. A. Zeb, K. Sabeeh, and M. Tahir, Chiral tunneling through a time-periodic potential in monolayer graphene, *Phys. Rev. B* **78**, 165420 (2008).
- [50] Z.-Z. Cao, Y.-F. Cheng, and G.-Q. Li, Massive Dirac electron tunneling through a time-periodic potential in single layer graphene, *Phys. Lett. A* **375**, 4065 (2011).
- [51] F. Sattari and S. Mirershadi, Tunneling time and transmission properties in strained graphene with a time-oscillating potential, *Phys. Scr.* **95**, 075702 (2020).
- [52] R. Jongchotanon and B. Soodchomshom, Nearly pure spin-valley sideband tunneling in silicene: Effect of interplay of time periodic potential barrier and spin-valley-dependent Dirac mass, *Physica E* **118**, 113950 (2020).
- [53] A. Jellal, M. Mekkaoui, E. B. Choubabi, and H. Bahlouli, Tunneling of massive Dirac fermions in graphene through time-periodic potential, *Eur. Phys. J. B* **87**, 123 (2014).
- [54] S. E. Savel'ev, W. Häusler, and P. Hänggi, Current Resonances in Graphene with Time-Dependent Potential Barriers, *Phys. Rev. Lett.* **109**, 226602 (2012).
- [55] L. Z. Szabó, M. G. Benedict, A. Czirják, and P. Földi, Relativistic electron transport through an oscillating barrier: Wave-packet generation and Fano-type resonances, *Phys. Rev. B* **88**, 075438 (2013).
- [56] H. Chen, Transmission in bilayer graphene through time-periodic potential, *Physica B* **456**, 167 (2015).
- [57] C. Schulz, R. L. Heinisch, and H. Fehske, Scattering of two-dimensional Dirac fermions on gate-defined oscillating quantum dots, *Phys. Rev. B* **91**, 045130 (2015).
- [58] U. Fano, Effects of configuration interaction on intensities and phase shifts, *Phys. Rev.* **124**, 1866 (1961).
- [59] J. Göres, D. Goldhaber-Gordon, S. Heemeyer, M. A. Kastner, H. Shtrikman, D. Mahalu, and U. Meirav, Fano resonances in electronic transport through a single-electron transistor, *Phys. Rev. B* **62**, 2188 (2000).
- [60] K. Kobayashi, H. Aikawa, S. Katsumoto, and Y. Iye, Tuning of the Fano Effect through a Quantum Dot in an Aharonov-Bohm Interferometer, *Phys. Rev. Lett.* **88**, 256806 (2002).
- [61] A. E. Miroshnichenko, S. Flach, and Y. S. Kivshar, Fano resonances in nanoscale structures, *Rev. Mod. Phys.* **82**, 2257 (2010).
- [62] W.-T. Lu, S.-J. Wang, W. Li, Y.-L. Wang, C.-Z. Ye, and H. Jiang, Fano-type resonance through a time-periodic potential in graphene, *J. Appl. Phys.* **111**, 103717 (2012).
- [63] N. Myoung, K. Seo, and G. Ihm, Demonstration of magnetic confinement in graphene with Fano-type resonances, *J. Korean Phys. Soc.* **62**, 275 (2013).
- [64] C. Zhang, J. Liu, and L. Fu, Anomalous Fano resonance of massive Dirac particle through a time-dependent barrier, *Europhys. Lett.* **110**, 61001 (2015).
- [65] H. H. Kh and E. Faizabadi, Dwell time, Hartman effect and transport properties in a ferromagnetic phosphorene monolayer, *J. Phys.: Condens. Matter* **30**, 085303 (2018).

- [66] C. Sinha and R. Biswas, Transmission of electron through monolayer graphene laser barrier, *Appl. Phys. Lett.* **100**, 183107 (2012).
- [67] V. A. Yampol'skii, S. Savel'ev, and F. Nori, Voltage-driven quantum oscillations in graphene, *New J. Phys.* **10**, 053024 (2008).
- [68] H. L. Calvo, H. M. Pastawski, S. Roche, and L. E. F. Foa-Torres, Tuning laser-induced band gaps in graphene, *Appl. Phys. Lett.* **98**, 232103 (2011).
- [69] G. Usaj, P. M. Perez-Piskunow, L. E. F. Foa Torres, and C. A. Balseiro, Irradiated graphene as a tunable Floquet topological insulator, *Phys. Rev. B* **90**, 115423 (2014).
- [70] P. M. Perez-Piskunow, L. E. F. Foa-Torres, and G. Usaj, Hierarchy of Floquet gaps and edge states for driven honeycomb lattices, *Phys. Rev. A* **91**, 043625 (2015).
- [71] J. Cayssol, B. Dóra, F. Simon, and R. Moessner, Floquet topological insulators, *Phys. Status Solidi RRL* **7**, 101 (2013).
- [72] K. Wintersperger, C. Braun, F. N. Ínal, A. Eckardt, M. D. Liberto, N. Goldman, I. Bloch, and M. Aidelsburger, Realization of an anomalous Floquet topological system with ultracold atoms, *Nat. Phys.* **16**, 1058 (2020).
- [73] Y. H. Wang, H. Steinberg, P. Jarillo-Herrero, and N. Gedik, Observation of Floquet-Bloch states on the surface of a topological insulator, *Science* **342**, 453 (2013).
- [74] F. Mahmood, C.-K. Chan, Z. Alpichshev, D. Gardner, Y. Lee, P. A. Lee, and N. Gedik, Selective scattering between Floquet-Bloch and Volkov states in a topological insulator, *Nat. Phys.* **12**, 306 (2016).
- [75] S. Afzal, T. J. Zimmerling, Y. Ren, D. Perron, and V. Van, Realization of Anomalous Floquet Insulators in Strongly Coupled Nanophotonic Lattices, *Phys. Rev. Lett.* **124**, 253601 (2020).
- [76] S. Longhi, Non-Hermitian Floquet invisibility, *Europhys. Lett.* **117**, 10005 (2017).
- [77] S.-J. Liang, S. Sun, and L. Ang, Over-barrier side-band electron emission from graphene with a time-oscillating potential, *Carbon* **61**, 294 (2013).
- [78] D. Sun, G. Aivazian, A. M. Jones, J. S. Ross, W. Yao, D. Cobden, and X. Xu, Ultrafast hot-carrier-dominated photocurrent in graphene, *Nat. Nanotechnol.* **7**, 114 (2012).
- [79] L. Tao, W. Ou, Y. Li, H. Liao, J. Zhang, F. Gan, and X. Ou, Recent advances in mechanical strain engineering of low-dimensional semiconductors and their applications in high-performance quantum emitters, *Semicond. Sci. Technol.* **35**, 103002 (2020).
- [80] V. M. Pereira, A. H. Castro Neto, and N. M. R. Peres, Tight-binding approach to uniaxial strain in graphene, *Phys. Rev. B* **80**, 045401 (2009).
- [81] V. M. Pereira and A. H. Castro Neto, Strain Engineering of Graphene's Electronic Structure, *Phys. Rev. Lett.* **103**, 046801 (2009).
- [82] V. M. Pereira, R. M. Ribeiro, N. M. R. Peres, and A. H. Castro Neto, Optical properties of strained graphene, *Europhys. Lett.* **92**, 67001 (2010).
- [83] R. M. Ribeiro, V. M. Pereira, N. M. R. Peres, P. R. Briddon, and A. H. C. Neto, Strained graphene: tight-binding and density functional calculations, *New J. Phys.* **11**, 115002 (2009).
- [84] G. Cocco, E. Cadelano, and L. Colombo, Gap opening in graphene by shear strain, *Phys. Rev. B* **81**, 241412(R) (2010).
- [85] F. M. D. Pellegrino, G. G. N. Angilella, and R. Pucci, Strain effect on the optical conductivity of graphene, *Phys. Rev. B* **81**, 035411 (2010).
- [86] S.-M. Choi, S.-H. Jhi, and Y.-W. Son, Effects of strain on electronic properties of graphene, *Phys. Rev. B* **81**, 081407(R) (2010).
- [87] G. G. Naumis, S. Barraza-Lopez, M. Oliva-Leyva, and H. Terrones, Electronic and optical properties of strained graphene and other strained 2D materials: a review, *Rep. Prog. Phys.* **80**, 096501 (2017).
- [88] I. I. Naumov and A. M. Bratkovsky, Gap opening in graphene by simple periodic inhomogeneous strain, *Phys. Rev. B* **84**, 245444 (2011).
- [89] H. Rostami and R. Asgari, Electronic ground-state properties of strained graphene, *Phys. Rev. B* **86**, 155435 (2012).
- [90] S. Barraza-Lopez, A. A. P. Sanjuan, Z. Wang, and M. Vanević, Strain-engineering of graphene's electronic structure beyond continuum elasticity, *Solid State Commun.* **166**, 70 (2013).
- [91] M. Assili, S. Haddad, and W. Kang, Electric field-induced valley degeneracy lifting in uniaxial strained graphene: Evidence from magnetophonon resonance, *Phys. Rev. B* **91**, 115422 (2015).
- [92] F. Guinea, M. I. Katsnelson, and A. K. Geim, Energy gaps and a zero-field quantum Hall effect in graphene by strain engineering, *Nat. Phys.* **6**, 30 (2009).
- [93] N. Levy, S. A. Burke, K. L. Meaker, M. Panlasigui, A. Zettl, F. Guinea, A. H. C. Neto, and M. F. Crommie, Strain-Induced Pseudo-Magnetic Fields Greater Than 300 Tesla in Graphene Nanobubbles, *Science* **329**, 544 (2010).
- [94] S. Haddad and L. Mandhour, Kohn anomaly of optical zone boundary phonons in uniaxial strained graphene: Role of the Dirac cone electronic dispersion, *Phys. Rev. B* **98**, 115420 (2018).
- [95] A. Contreras-Astorga, V. Jakubský, and A. Raya, On the propagation of Dirac fermions in graphene with strain-induced inhomogeneous Fermi velocity, *J. Phys.: Condens. Matter* **32**, 295301 (2020).
- [96] Y. Zahidi, I. Redouani, A. Jellal, and H. Bahloul, Magnetic field effect on strained graphene junctions, *Physica E* **115**, 113672 (2020).
- [97] Y. Concha, A. Huet, A. Raya, and D. Valenzuela, Supersymmetric quantum electronic states in graphene under uniaxial strain, *Mater. Res. Express* **5**, 065607 (2018).
- [98] S.-M. Lee, S.-M. Kim, M. Y. Na, H. J. Chang, K.-S. Kim, H. Yu, H.-J. Lee, and J.-H. Kim, Materialization of strained CVD-graphene using thermal mismatch, *Nano Res.* **8**, 2082 (2015).
- [99] D. Midtvedt, C. H. Lewenkopf, and A. Croy, Strain-displacement relations for strain engineering in single-layer 2D materials, *2D Mater.* **3**, 011005 (2016).
- [100] J. C. Pérez-Pedraza, E. Díaz-Bautista, A. Raya, and D. Valenzuela, Critical behavior for point monopole and dipole electric impurities in uniformly and uniaxially strained graphene, *Phys. Rev. B* **102**, 045131 (2020).
- [101] Z. Wu, F. Zhai, F. M. Peeters, H. Q. Xu, and K. Chang, Valley-Dependent Brewster Angles and Goos-Hänchen Effect in Strained Graphene, *Phys. Rev. Lett.* **106**, 176802 (2011).
- [102] M. C. Rechtsman, J. M. Zeuner, A. Tünnermann, S. Nolte, M. Segev, and A. Szameit, Strain-induced pseudomagnetic field and photonic Landau levels in dielectric structures, *Nat. Photonics* **7**, 153 (2012).

- [103] T. Stegmann and N. Szpak, Current flow paths in deformed graphene: from quantum transport to classical trajectories in curved space, *New J. Phys.* **18**, 053016 (2016).
- [104] T. Stegmann and N. Szpak, Current splitting and valley polarization in elastically deformed graphene, *2D Mater* **6**, 015024 (2019).
- [105] J. J. Wang, S. Liu, J. Wang, and J. F. Liu, Valley-coupled transport in graphene with Y-shaped Kekulé structure, *Phys. Rev. B* **98**, 195436 (2018).
- [106] J. J. Wang, S. Liu, J. Wang, and J. F. Liu, Valley supercurrent in the Kekulé graphene superlattice heterojunction, *Phys. Rev. B* **101**, 245428 (2020).
- [107] Y. Betancur-Ocampo, Partial positive refraction in asymmetric Veselago lenses of uniaxially strained graphene, *Phys. Rev. B* **98**, 205421 (2018).
- [108] S.-H. Zhang and W. Yang, Anomalous caustics and Veselago focusing in 8-Pmmn borophene p–n junctions with arbitrary junction directions, *New J. Phys.* **21**, 103052 (2019).
- [109] L. Tarruell, D. Greif, T. Uehlinger, G. Jotzu, and T. Esslinger, Creating, moving and merging Dirac points with a Fermi gas in a tunable honeycomb lattice, *Nature (London)* **483**, 302 (2012).
- [110] O. Bahat-Treidel, O. Peleg, M. Grobman, N. Shapira, M. Segev, and T. Pereg-Barnea, Klein Tunneling in Deformed Honeycomb Lattices, *Phys. Rev. Lett.* **104**, 063901 (2010).
- [111] E. Cadelano, P. L. Palla, S. Giordano, and L. Colombo, Non-linear Elasticity of Monolayer Graphene, *Phys. Rev. Lett.* **102**, 235502 (2009).
- [112] C. Lee, X. Wei, J. W. Kysar, and J. Hone, Measurement of the Elastic Properties and Intrinsic Strength of Monolayer Graphene, *Science* **321**, 385 (2008).
- [113] H. H. P. Garza, E. W. Kievit, G. F. Schneider, and U. Stauffer, Controlled, reversible, and nondestructive generation of uniaxial extreme strains (>10%) in graphene, *Nano Lett.* **14**, 4107 (2014).
- [114] J.-H. Wong, B.-R. Wu, and M.-F. Lin, Strain effect on the electronic properties of single layer and bilayer graphene, *J. Phys. Chem. C* **116**, 8271 (2012).
- [115] M. I. Katsnelson, K. S. Novoselov, and A. K. Geim, Chiral tunnelling and the Klein paradox in graphene, *Nat. Phys.* **2**, 620 (2006).